Acta Crystallographica Section A
Foundations of Crystallography
ISSN 0108-7673

Received 23 December 1999
Accepted 3 March 2000

Diffuse X-ray scattering and disorder in *p*-methyl-*N*-(*p*-chlorobenzylidene)aniline, $C_{14}H_{12}ClN$ (ClMe): analysis *via* automatic refinement of a Monte Carlo model

T. R. Welberry

Research School of Chemistry, Australian National University, Canberra, ACT 0200, Australia. Correspondence e-mail: welberry@rsc.anu.edu.au

A recently developed method for fitting a Monte Carlo computer simulation model to observed single-crystal diffuse X-ray scattering has been applied to (*h*0*l*) scattering data obtained for the disordered compound *p*-methyl-*N*-(*p*-chlorobenzylidene)aniline, $C_{14}H_{12}ClN$ (ClMe), at 295 K. Each molecular site is occupied by a molecule in one of four basically different orientations defined by combinations of a side-to-side and an end-to-end flip. These different orientations were represented in the model by two sets of binary random variables. In addition to these occupancy variables, the model also allowed local orientational and centre-of-mass translational displacements. The disordered structure was modelled using rigid-body molecules linked by harmonic springs to represent 'effective' intermolecular interactions. The refined model included 4 parameters describing the correlation of neighbouring occupational variables and 28 parameters describing the force-constant and 'size-effect' parameters on seven symmetry-inequivalent types of intermolecular vectors. The model refined to an overall agreement factor, $R = [\sum w(\Delta I)^2 / \sum wI_{obs}^2]^{1/2}$, of 32.8% for 28500 data points. It was found that the SRO correlation structure observed within the layers of molecules in the *ab* plane is typical of a frustrated lattice, where nearest- and second-nearest-neighbour effects oppose each other. This appears to be the main difference between this compound and the sister compound, *p*-chloro-*N*-(*p*-methylbenzylidene)aniline (MeCl), studied previously. The local relaxational displacements that result from local 'size-effect' strains operating on different intermolecular vectors generally reflect the tendency for distances involving Cl—Cl interactions to be longer than the observed average distances.

1. Introduction

The present investigation is part of a long-term study of diffuse scattering from disordered crystals in which we attempt to understand and explain the origins of the disorder in terms of basic interatomic or intermolecular interactions. The pair of disordered compounds, MeCl, *p*-chloro-*N*-(*p*-methylbenzylidene)aniline (I) and ClMe, *p*-methyl-*N*-(*p*-chlorobenzylidene)aniline (II) makes a particularly interesting system for study.

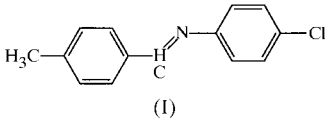

(I)

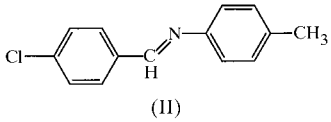

(II)

The two compounds are isostructural, since they differ only in the disposition of the —CH═N— linkage joining the two phenyl ring systems (see Bar & Bernstein, 1983, Haller *et al.*, 1995). However, both give strong and richly detailed diffuse X-ray diffraction patterns (see Fig. 1). Though showing some similarity, these patterns are nevertheless quite distinct, indicating substantially different local ordering schemes. A second point of interest in these compounds is that a given molecular site in the crystal is occupied by one of *four* basically different orientations of the molecule. A further degree of complexity is afforded by the fact that the molecules have internal flexibility, which has the potential of affecting local strain relaxation processes arising from the disorder.

Of the two compounds, MeCl gives a diffraction pattern that is rather simpler to understand. In particular, the short-range-order (SRO) diffraction peaks labelled *S* in Fig. 1(*a*) are all of a similar symmetric shape, while the same peaks for ClMe vary from symmetric elongated peaks labelled *E* to shorter more asymmetric peaks labelled *A*. In a previous

paper (Welberry *et al.*, 1993; see also Welberry & Butler, 1994), we reported a study of the diffuse X-ray scattering from MeCl. In that work, the four basic molecular orientations were represented in a two-dimensional Monte Carlo computer model by two sets of binary random variables, $\sigma_{i,j}$ and $\rho_{i,j}$, $\sigma_{i,j}$ representing the effect of flipping the molecules end-to-end and $\rho_{i,j}$ representing a side-to-side flip. Further continuous random variables $U_{i,j}$ and $V_{i,j}$ (Gaussian) were used to model the rigid-body displacements of the molecules parallel and perpendicular to the long axis of the molecule. By introducing correlations into these arrays of random variables, a model was established that was able to account, at least qualitatively, for most of the diffuse diffraction features that may be seen in Fig. 1(*a*).

One limitation of this earlier work was that the four sets of random variables describing the different disorder effects were considered to be independent – a rather drastic assumption, but one for which there did not appear to be a great deal of counter evidence. Only one or two rather weak diffuse peaks, labelled *G* in Fig. 1(*a*), which could not be accounted for by the simple model, gave any suggestion that interactions (cross-correlations) between the different variables might be important. A second limitation of this work was that the model, formulated as it was in terms of correlations in the arrays of random variables, did not focus on the underlying physical reasons for these correlations. So while this type of modelling was able to give some insight into how the molecules in MeCl move relative to each other as a result of the disorder, the overall description could not be considered completely satisfactory. In addition, it was clear that this simple approach could not cope effectively with the more complex diffuse scattering exhibited by ClMe.

More recently, however, the advent of cheaper and faster computing has led to a considerable enhancement of our ability to analyse and model such diffuse X-ray patterns. In particular, we have developed a means of fitting a suitably parameterized Monte Carlo model to the observed X-ray data using least-squares refinement (Welberry *et al.*, 1998). First the model is set up in terms of basic interactions between atoms or molecules, taking into account the average structure as revealed by Bragg analysis, and allowing for the fact that intermolecular or interatomic distances will depend on the details of the local occupational ordering. Parameters specifying these interactions are then iteratively adjusted until a good agreement is obtained between the observed diffraction patterns and ones calculated from the model coordinates. At each stage of the refinement, a goodness-of-fit parameter χ^2 is used as a quantitative measure of the agreement of the model diffraction pattern with the observed data:

$$\chi^2 = \sum_{h,k,l,m} w_{hklm}\{\Delta I\}^2, \qquad (1)$$

where

$$\Delta I = I_{\rm obs} - (b_m + f_m I_{\rm calc}). \qquad (2)$$

Here, the summation is over all non-integral reciprocal points h, k, l corresponding to individual pixels in the m measured sections of data. f_m is a scale and b_m a backgound correction applied to section m. [Note that b_m and f_m are determined as described in Proffen & Welberry (1997) and are not included as variables in the least-squares matrix.] w_{hklm} is the weight for the corresponding data point h, k, l of data plane m. The weights used in the work described here were taken as $w_{hklm} = 1/I_{\rm obs}$. Numerical estimates of the differentials of χ^2 with respect to the model parameters are calculated by performing additional simulations in which each parameter in turn has been incremented by a small amount. These differentials are then used to form the least-squares matrix and provide automatic updating of the parameters before the next iteration.

This methodology is very computer intensive and is only just becoming a viable means of analysis with the advent of very fast and inexpensive workstations, and even then cannot be used without some simplification of the problem. In the present paper, we apply these new methods to a study of the disorder in ClMe. With four different molecular orientations possible in a given site, and each molecule being in direct contact with 14 neighbours, this represents a considerable step up in complexity from the simple iron carbonyl study (Welberry *et al.*, 1998). Consequently, here too, simplifications have had to be made. These are described in detail in §3.

The computational resources required for this new methodology are formidable and depend on a number of factors. The calculations are in two stages: the Monte Carlo simulation and the subsequent calculation of diffraction patterns. For the Monte Carlo simulation, the time for a calculation depends on the system size and the number of MC iterations carried out. For the calculation of the diffraction pattern, the time depends on the number of reciprocal sections, the number of reciprocal points per section at which calculations are made and the quality of calculation performed (by quality we mean high resolution and low noise). In the present study, in order to minimize the computation time required, we limited our attention to the single section of data, (*h*0*l*), shown in Fig. 1(*b*). This section corresponds to the projection of the structure down the *b* axis in which all the molecules are well resolved (see Fig. 3*a*) and contains most of the interesting detail in the diffraction pattern. The MC simulation, however, was performed in three dimensions and it was necessary to apply some constraints to the modelling procedure to avoid the use of parameters that could not be resolved in this single view of the structure.

2. Experimental data

The diffuse scattering data for MeCl and ClMe shown in Figs. 1(*a*) and 1(*b*), respectively, were recorded using the position-sensitive-detector (PSD) system described by Osborn & Welberry (1990). This system uses a flat-cone Weissenberg geometry, which allows a complete section of data to be recorded with a single stationary setting of the PSD while the crystal is rotated through 360° in 1000 steps of 0.36° in ω. The raw data are obtained as a two-dimensional array of points in the Weissenberg space (2θ *versus* ω). Before use, these are

rebinned into a square array of points, most usually 400 × 400 pixels, in the undistorted reciprocal-lattice plane. At this scale, the experimental resolution due to beam divergence, crystal size and mosaic spread then corresponds approximately to a single pixel in this plane. Each data point is renormalized by dividing by the number of raw data points contributing to it, so that no correction due to the Lorenz effect is required. In the present case, corrections due to X-ray polarization and specimen absorption were neglected. Graphite-monochromated Cu$K\alpha$ ($\lambda = 1.5418$ Å) radiation was used. Though the measured data are obtained and used in digital form, it is convenient for comparison purposes to display the data as false-colour or grey-scale images, as shown in Fig. 1.

The images shown in Fig. 1, which contain 160000 data points, are excessively large for the direct-fitting methodology described above. In the case of the $Fe_3(CO)_{12}$ study mentioned earlier, the number of data used was kept within reasonable bounds by selecting specific small areas from the data that appeared to contain the most useful information, while retaining the experimental spatial resolution. For the present study, we opted instead to utilize the whole section of data and reduced the number of data points by rebinning the data to form a more manageable but lower-resolution array of 200 × 200 pixels.

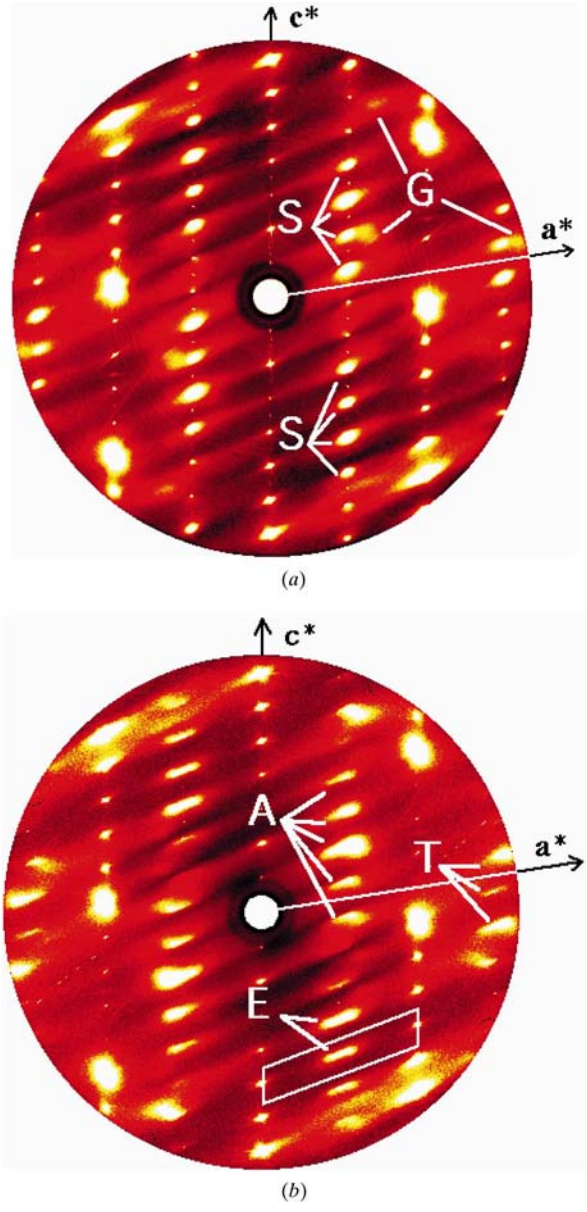

Figure 1
X-ray diffraction patterns ($h0l$ section) for (*a*) MeCl, (*b*) ClMe. The labelled features are referred to in the text.

3. Monte Carlo model

3.1. Geometry considerations

The average structure determination (Haller *et al.*, 1995) revealed that the true space group of ClMe is $P2_1/n$ on a unit cell with $a = 5.971$, $b = 7.411$, $c = 27.420$ Å, $\beta = 99.13^\circ$. However, the structure is very close to being $P2_1/a$ on a cell of half the c spacing (as reported earlier by Bar & Bernstein, 1983) and in the present work we assume this simpler cell, in which there are two molecules only.

The coordinates for each of the four possible orientations of the ClMe molecule in a given site were taken directly from the crystal structure refinement of Haller *et al.* (1995) and referred to a local (molecular) orthonormal coordinate system with axes X', Y' and Z', which were taken as the principal axes of the inertia tensor of the average molecule. These four different orientations are each shown in Fig. 2 together with a plot of the average. Although, as stated earlier, the MeCl and ClMe molecules have internal flexibility – the possibility of each phenyl ring rotating around the single bonds of the —CH═N— linkage – for the present paper, we assume that this internal degree of freedom is relatively unimportant and the molecules may to a good approximation be treated as rigid bodies. Consequently, the actual molecular coordinates featuring in Fig. 2 were used only to calculate the diffraction patterns from the MC results. At all intermediate stages in the computer simulation, the molecules were represented as a four-point plane cross-shaped motif (shown in black in Fig. 2), which defines the principal axes X', Y' and Z' of the molecular site.

The position and orientation of the molecular entity in any molecular site were defined by three centre-of-mass coordinates $x_{p,q,r,s}$, $y_{p,q,r,s}$, $z_{p,q,r,s}$ and two orientational variables $\varphi1_{p,q,r,s}$ and $\varphi2_{p,q,r,s}$, which defined local rotations away from the mean orientation around the X' and Z' molecular axes. The four indices, p, q, r, s, comprise three indices to label the particular unit cell and one to specify the molecular site within the cell. In view of the fact that the refinement reported here used the ($h0l$) section data only, rotations about Y' were constrained to be zero, since small rotations about this axis would mainly affect the y coordinates and would not be detectable in projection down **b**.

3.2. Monte Carlo simulation

We have found in previous studies that in order to obtain a computed diffraction pattern from a Monte Carlo simulation

Table 1
Definitions of the 26 different intermolecular vectors used in the MC simulations.

The vectors are from a reference molecule defined by the four integers (0001) to the molecular sites given in column 2. The first three integers define the unit cell and the fourth the molecular site within the cell. Column 3 gives details of which pseudoatoms of the molecular motif are involved in each contact. Column 4 enumerates the 14 different neighbouring molecules with which the reference molecule is in contact. Column 5 lists the different constants used for introducing occupancy correlations along the different vectors. Column 6 gives the spring constant used for inducing relaxational displacements on each vector. Column 7 gives the average equilibrium distance for each vector. Column 8 gives the random variables that are used to induce 'size-effect' distortions on each vector.

Vector	To molecule at site	Pseudoatom contacts	Neighbour number	Occupancy correlation constant	Spring constant	Equilibrium distance	Size effect dependent on
1	$\bar{1}011$	2–1	1	J_1	K_1	3.595	$\sigma_{p,q,r,s}$
2	$10\bar{1}1$	1–2	2				
3	0011	2–1	3	J_2	K_2	4.126	$\sigma_{p,q,r,s}$
4	$00\bar{1}1$	1–2	4				
5	$\bar{1}002$	3–4	5	J_3	K_3	4.250	$\rho_{p,q,r,s}$
6	$\bar{1}102$	3–4	6				
7	0102	4–3	7				
8	0002	4–3	8				
9	$\bar{1}012$	2–1	9	J_4	K_4	4.438	$\sigma_{p,q,r,s}$
10	$\bar{1}112$	2–1	10				
11	$01\bar{1}2$	1–2	11				
12	$00\bar{1}2$	1–2	12				
13	$\bar{1}102$	1–1	6	J_3	K_5	4.514	$\sigma_{p,q,r,s}$
14	$\bar{1}002$	2–2	5				
15	0102	1–1	7				
16	0002	2–2	8				
17	$\bar{1}102$	2–2	6	J_3	K_6	5.011	$\sigma_{p,q,r,s}$
18	$\bar{1}002$	1–1	5				
19	0102	2–2	7				
20	0002	1–1	8				
21	$\bar{1}001$	3–4	13	J_5	K_7	5.058	$\rho_{p,q,r,s}$
22	1001	4–3	14				
23	$\bar{1}001$	1–1	13	J_5	K_8	5.971	$\sigma_{p,q,r,s}$
24	$\bar{1}001$	2–2	13				
25	1001	1–1	14				
26	1001	2–2	14				

that is of sufficient quality (high resolution, low noise) to allow comparison with the observed data, a simulation size of at least $32 \times 32 \times 32$ unit cells is required. In the present case, it was decided, since only the $h0l$ data was to be used, to extend the size in the a and c directions and correspondingly reduce the dimension in the b direction. In the present study, therefore, the simulation size was $64 \times 8 \times 64$ with two molecular sites per cell making a total of 65536 molecules or 1048526 atoms.

Diffraction patterns were calculated from the output of each MC run using the program *DIFFUSE* (Butler & Welberry, 1992). This obtains the calculated diffuse diffraction pattern by averaging the diffraction patterns obtained from a large number of subregions (lots) taken at random from the total simulation array. In the present case, 100 individual lots of $16 \times 3 \times 7$ unit cells were used. Calculations were made on the same 200×200 grid as used for the observed data. The total CPU time for a single calculated pattern using these specifications was ~40 min on a single 400 MHz Pentium II processor.

3.3. Occupancy variables

The occupancy of a given site was defined in terms of the same two binary random variables, $\sigma_{p,q,r,s}$ and $\rho_{p,q,r,s}$, used in the MeCl study. The four orientations of the molecules relative to the local orthonormal coordinates shown in Fig. 2(*b*) corresponded to the values of $\sigma_{p,q,r,s}$ and $\rho_{p,q,r,s}$. Correlations were introduced into these random-variable arrays by performing two separate MC simulations. First, correlations were introduced into the $\rho_{p,q,r,s}$ variables, representing side-to-side disorder, using a MC energy of the form

$$E_{SS} = \sum_{\text{all nearest neighbours}} J_m \rho_n \rho_m. \tag{3}$$

Here, n stands for the point p,q,r,s and m for a nearest-neighbouring point and the summation is over all such nearest-neighbouring vectors. J_m are interaction constants applicable to each symmetry-independent type of neighbouring vector (see Table 1 for defintions). The form of the equation assumes that the $\rho_{p,q,r,s}$ are $(-1, +1)$ binary random variables. In practice, it is often convenient to use $(0, 1)$ random variables, σ' and ρ', which are entirely equivalent to the $(-1, +1)$ variables σ and ρ *via* the simple transformation

$$\rho' = \tfrac{1}{2}(1 + \rho), \quad \sigma' = \tfrac{1}{2}(1 + \sigma). \tag{4}$$

In the following sections, whenever the variables are used in equations the $(-1, 1)$ definition applies, but at other times it is often convenient to use the $(0, 1)$ description.

Geometry calculations show that each molecule is in direct contact with 14 neighbouring molecules made up of 7 pairs of symmetry-related vectors. Consequently, 7 independent J_m constants need to be specified. In fact, in the MC simulation, it has been found convenient, and is our usual practice, to iteratively adjust the values of the J_m constants in order to produce given values of the correlation coefficients (or SRO parameters), C_m, along each vector from a given point n to its neighbouring point m, where C_m is defined as

$$C_m = \langle \rho_n \rho_m \rangle - \langle \rho_n \rangle \langle \rho_m \rangle. \tag{5}$$

These correlation coefficients or SRO parameters then become part of the set of system parameters that need to be determined during the analysis.

A second similar set of 7 correlation coefficients was then introduced into the array of the $\sigma_{p,q,r,s}$ variables using the same interaction vectors. However, here an additional term E_{EESS} was inserted into the MC energy in order to introduce a cross-correlation between the $\sigma_{p,q,r,s}$ and $\rho_{p,q,r,s}$ variables. In this case, the MC energy was then of the form

$$E_{EE} + E_{EESS} = \sum_{\text{all nearest neighbours}} J_m \sigma_n \sigma_m + \kappa \sigma_n \rho_n. \qquad (6)$$

κ is an interaction parameter used to introduce the cross correlation. The value of κ was determined during the least-squares fitting. 50 cycles of MC iteration were used for each of the two stages of occupancy variable ordering.

3.4. Displacement variables

Although semi-empirical atom–atom potentials are well developed for molecular crystals and could be expected to give a good representation of real intermolecular interactions, the use of such a detailed potential in a Monte Carlo simulation would be far too time consuming to be contemplated with current computational resources, when it is necessary to have a simulation size large enough to ensure that statistical parameters are reasonably accurately represented. Consequently, we use instead the notion of *effective* interactions. In this work, the interactions of a given molecule with its neighbours are modelled by placing simple harmonic springs between the four points of the molecular motif shown in Fig. 3, and corresponding points in neighbouring motifs. In some cases, only a single spring is used but for some interactions two or three separate springs are required in order to account for the possibility of rotational motion. Thus, for the same 14 nearest-neighbour vectors used for the occupancy variables, we used 26 connecting springs. The intermolecular vectors along which these springs are placed are listed in Table 1 and are also shown schematically in Fig. 3(*b*).

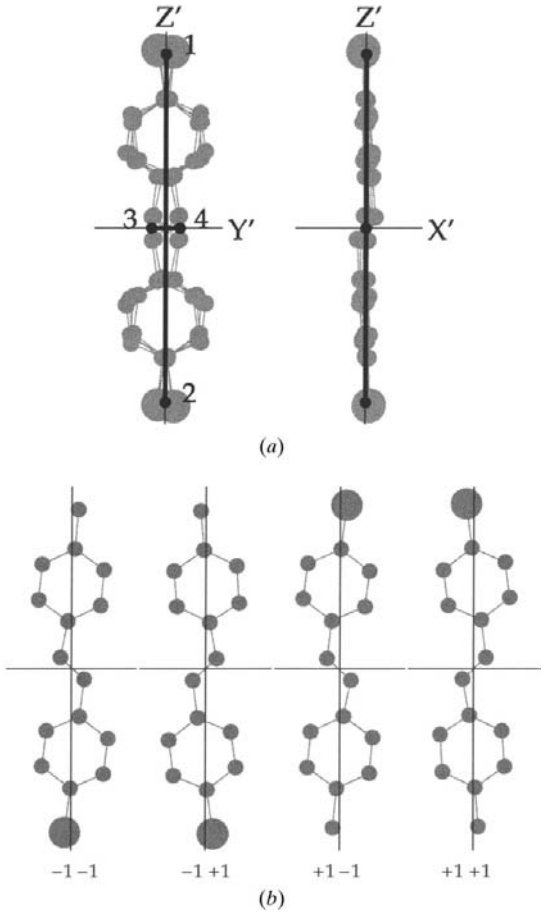

Figure 2
(*a*) The average molecular site showing the local axial system X', Y', Z' and the cross-shaped motif defined by the four pseudoatoms (small black circles) that is used in the MC simulations. (*b*) The four different orientations of the molecule together with the values of the σ and ρ random variables that define them.

The atomic or molecular displacements that occur in a nondisordered crystal are due to thermal motion and, if the resulting thermal diffuse scattering (TDS) were modelled using the Monte Carlo simulation techniques described here, we would need to ensure that the set of springs used to model the effective interactions were capable of correctly describing this TDS. In the present case, however, the displacements that are present in the crystals are induced almost entirely as a result of local relaxation accompanying the occupational disorder, as witnessed by the fact that the observed diffuse X-ray patterns change very little as the temperature is reduced to ~100 K. Thus, while we might expect the strength (force constants) of the springs to reflect basically the same interactions that give rise to TDS in an ordered crystal, the major effect in inducing the displacements is undoubtedly the different preferred contact distances (spring lengths) that will occur as a result of the different mutual orientations of the two connected molecules. We generally refer to this local strain induction as the 'size effect' by analogy with the original concept of the 'size effect' in alloys (see Warren *et al.*, 1951).

3.5. Size-effect strain

We can represent the energy for the size-effect strain as

$$E_{\text{size}} = \sum_{\text{all vectors}} K_m [d_{n,m} - d_{\text{ave}}(1 + \varepsilon_{n,m})]^2. \qquad (7)$$

Here, K_m is the spring constant corresponding to the vector joining the given site n and a neighbouring site m (see Table 1). $d_{n,m}$ is the instantaneous length of this vector and d_{ave} its observed average length. The size-effect parameter $\varepsilon_{n,m}$ depends on the values of σ and ρ at sites n and m. In the present case, for each of the 26 vectors, there are in principle 16 different combinations of the orientations of the two molecules in the sites n and m, and consequently 16 different values for the size-effect parameters $\varepsilon_{n,m}$. Although there are some necessary constraints on the values these parameters may take in order that the average intermolecular spacing is maintained and symmetry requirements satisfied, use of such a large number of variables is simply not feasible and we must look for suitable simplifications.

The simplification we have adopted in the present work is that the vectors involving contacts at the ends of the molecular motifs (*i.e.* involving pseudoatoms 1 and 2) have size-effect parameters that are dependent only on the σ variables and the vectors involved with contacts at the centres of the molecular motifs (pseudoatoms 3 and 4) have size-effect parameters that are dependent only on the ρ variables. This dependency is summarized in the rightmost column of Table 1. Then, for each vector, we can specify the size-effect parameters in terms of only four variables $\varepsilon_{0,0}$, $\varepsilon_{0,1}$, $\varepsilon_{1,0}$, $\varepsilon_{1,1}$. Here for convenience the subscripts refer to the (0, 1) description of the binary variable defined in equation (4). It should be noted that there is redundancy in these four variables since, in order to maintain the average distance,

$$P_{0,0}\varepsilon_{0,0} + P_{0,1}\varepsilon_{0,1} + P_{1,0}\varepsilon_{1,0} + P_{1,1}\varepsilon_{1,1} = 0. \qquad (8)$$

$P_{0,0}$ is, for example, the probability that the two molecules are in orientations corresponding to $\sigma'_n = 0$ and $\sigma'_m = 0$ (or $\rho'_n = 0$ and $\rho'_m = 0$). These probabilities are related to the site occupancy m_1 and the occupational correlations C_m along the same vector by

$$C_m = (P_{1,1} - m_1^2)/[m_1(1 - m_1)]. \qquad (9)$$

In the analysis, we use $\varepsilon_{0,0}$, $\varepsilon_{0,1}$ and $\varepsilon_{1,0}$ as variables and set

$$\varepsilon_{1,1} = -(P_{0,0}\varepsilon_{0,0} + P_{0,1}\varepsilon_{0,1} + P_{1,0}\varepsilon_{1,0})/P_{1,1}, \qquad (10)$$

giving three independent size-effect variables per vector. It should be noted that symmetry-related vectors, such as, say, vectors 1 and 2, require the same set of four size-effect parameters, $\varepsilon_{0,0}$, $\varepsilon_{0,1}$, $\varepsilon_{1,0}$ and $\varepsilon_{1,1}$, but their order is changed to take account of the fact that, if all molecules are in orientation (0), vector 1 involves contact between pseudoatoms 1 and 2 while vector 2 involves contact between pseudoatoms 2 and 1. Therefore, $\varepsilon_{0,0}$, $\varepsilon_{0,1}$, $\varepsilon_{1,0}$ and $\varepsilon_{1,1}$ for vector 1 become $\varepsilon_{1,1}$, $\varepsilon_{1,0}$, $\varepsilon_{0,1}$ and $\varepsilon_{0,0}$, respectively, for vector 2.

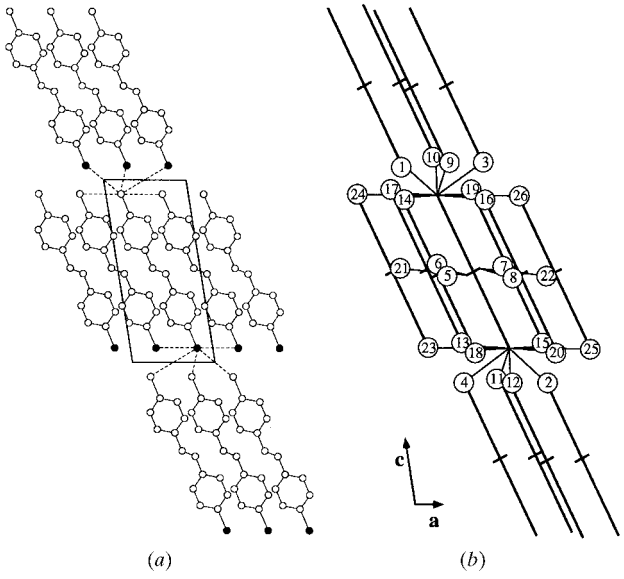

Figure 3
(*a*) Plot of the structure of ClMe viewed down **b**. In this figure, all molecules are shown in the orientation corresponding to $\sigma = -1$, $\rho = -1$. The unit cell shown is that used in the MC simulations. (*b*) Schematic diagram of the environment of a central molecule of ClMe showing the 26 different vectors (thin lines) along which 'springs' linking the central molecule to its 14 neighbours are placed to represent the effective intermolecular interactions. The view here is slightly rotated relative to (*a*) to reveal superimposed neighbours. The heavy lines represent the cross-shaped molecular motif referred to in the text. See also Table 1.

4. Results

4.1. Occupational correlations

In a previous study of the iron carbonyl compound $Fe_3(CO)_{12}$, we adopted the strategy of first refining a set of occupational correlations using only regions of the data that appeared little affected by displacement disorder and then subsequently refining a model that described the size-effect-like local relaxations. For the present study, where substantially more computational resources and a complete reciprocal-lattice section of data were available, attempts were made to refine all variables simultaneously. However, it soon became apparent that it was all too easy for the displacement variables to attempt to spuriously make a fit to the short-range-order peaks. The resulting fits were unstable and gave widely varying SRO parameter values and poorly reproduced SRO peak shapes. Consequently, it was decided to revert to the previous strategy.

In the study of MeCl, it was concluded that there did not appear to be any evidence for correlations in the side-to-side disorder and the distribution of the $\rho_{p,q,r,s}$ variables was therefore assumed to be random throughout. This assumption was initially also made in the present case for ClMe. In order to obtain correlations for the $\sigma_{p,q,r,s}$ variables, we used the small region of data containing the most symmetric elongated SRO peak enclosed by the white parallelogram in Fig. 1(*b*). The marked asymmetry of the SRO peaks labelled *A* is indicative that these peaks are substantially affected by relaxational displacement. Of the five symmetry-inequivalent constants J_i defined in Table 1, it was found that only three, J_3, J_4 and J_5, were required to model this elongated symmetric peak shape satisfactorily. The values of the correlation coefficients (corresponding to these interactions) that were determined as giving the best fit to this peak were $C_3 = -0.50$, $C_4 = +0.225$, $C_5 = +0.17$. A calculated diffraction pattern obtained from a MC simulation using these values for the $\sigma_{p,q,r,s}$ variables only, and with no subsequent displacements allowed, is shown in Fig. 4(*a*). It may be readily seen that the same basic peak shape is reproduced for all SRO peaks.

By comparing Fig. 4(*a*) with the observed pattern, however, it may be seen that using this correlation structure for the $\sigma_{p,q,r,s}$ variables alone results in two features that are not modelled well. First, the region between the columns of SRO peaks clearly contains bands of diffuse scattering that connect the peaks in the $0.5\mathbf{a}^*$ column with ones in the $1.5\mathbf{a}^*$ column. Secondly, the relative intensities of the three strongest diffuse peaks in the $1.5\mathbf{a}^*$ column do not agree with corresponding

peaks in the observed pattern (labelled T in Fig. 1b). In the observed pattern, the middle of the three is considerably weaker than the outer two. These two features led us to consider that non-zero $\rho_{p,q,r,s}$ correlations must also exist. In particular, the first feature mentioned above implies that the $\rho_{p,q,r,s}$ variables must also be negatively correlated along the vector corresponding to J_3. Similarly, test calculations also indicated that in the c^* direction the $\rho_{p,q,r,s}$ variables must also be correlated in a manner similar to the $\sigma_{p,q,r,s}$ variables. However, attempts to refine correlation values for the $\rho_{p,q,r,s}$ variables, independently of those for the $\sigma_{p,q,r,s}$ variables, were unsuccessful. We attribute this to the fact that no clearly defined SRO peak existed in the data that could be exclusively attributed to $\rho_{p,q,r,s}$ correlations. In the absence of any further evidence, a model was adopted in which the target values for the correlations in the two arrays were assumed to be the same. Since the two arrays have different site occupancies, however, the actual correlation values realized, though similar, were somewhat different. Final values for the correlations on the two arrays are given in Table 2. This model for the occupancy correlations was then used throughout the remaining analysis. A calculated diffraction pattern obtained from a MC simulation using this model, with no subsequent displacements allowed, is shown in Fig. 4(*b*). Note the absence of fringes between the columns of SRO peaks. The relative intensity of the peaks indicated as T in Fig. 1(*b*) is somewhat improved, although the enhancement of the intensity of the next SRO peak in the column is indicative of the fact that there may still be some residual problem with this part of the model.

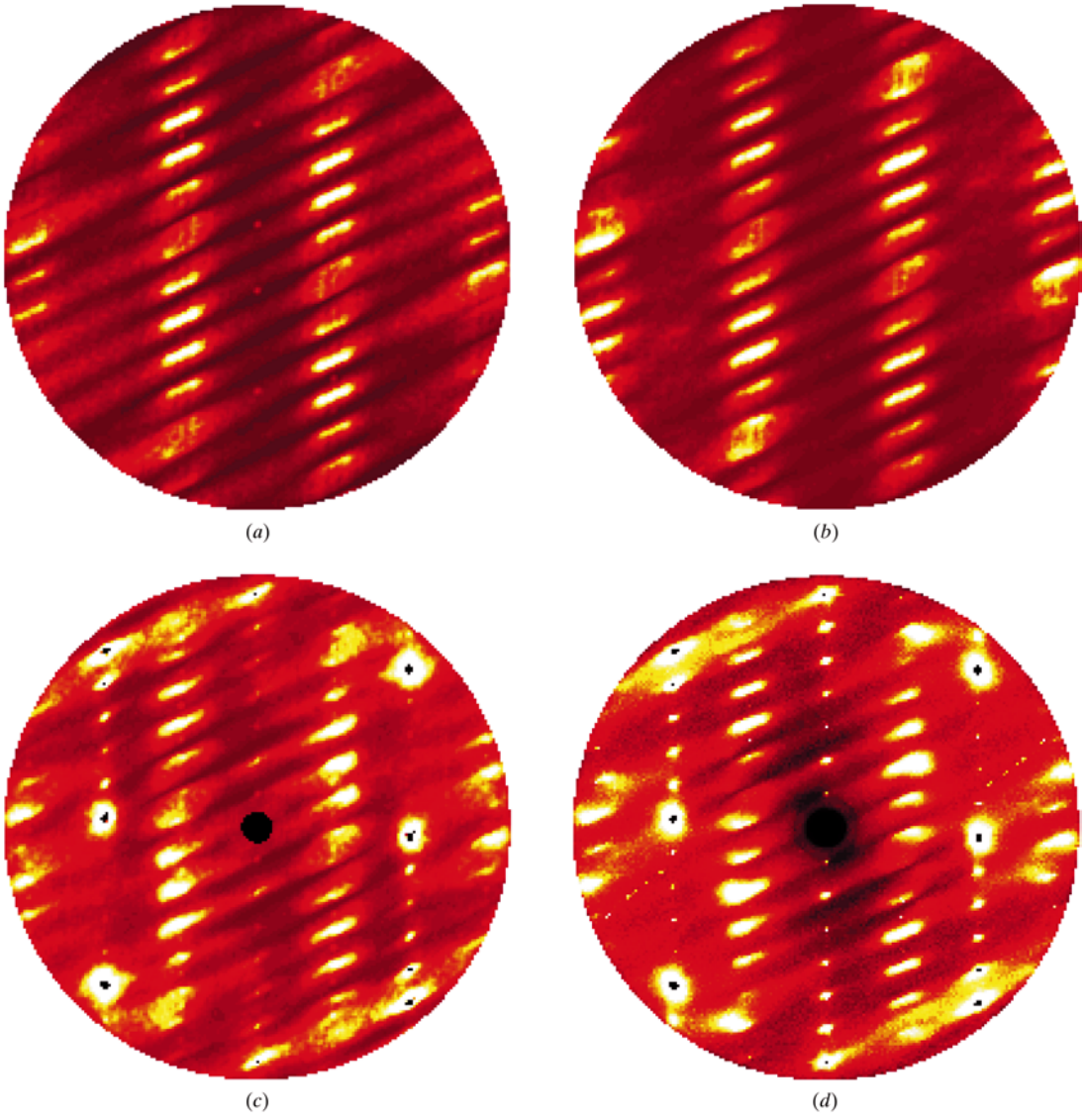

Figure 4
Diffraction patterns calculated from the Monte Carlo simulation. (*a*) Using occupancy correlations for the end-to-end disorder, zero correlations for the side-to-side disorder and no displacements. (*b*) Using occupancy correlations for both end-to-end and side-to-side disorder and no displacements. (*c*) Final calculated diffraction pattern including side-to-side correlations, end-to-end correlations, a cross-correlation between these two, and size-effect relaxation displacements. (*d*) Observed X-ray data for comparison.

The only additional feature included in subsequent work that affected the occupancy variables was a parameter that allowed cross-correlation between the $\rho_{p,q,r,s}$ and the $\sigma_{p,q,r,s}$ variables. Initially, the $\rho_{p,q,r,s}$ and $\sigma_{p,q,r,s}$ variables were assumed independent so that the proportions of the four different molecular orientations shown in Fig. 2(*b*) were 0.35:0.15:0.35:0.15 in accordance with the site occupancies determined by the Bragg reflection structure determination. During the final least-squares refinement, it was found that $\rho_{p,q,r,s}$ and $\sigma_{p,q,r,s}$ became highly correlated, so much so that the occupancies of the four orientations became 0.50:0.00:0.2:0.3, respectively. This may be reconciled with the Bragg experiment if the determined structure occurs in two twin domains related by a twofold axis so that the average occupancies arise from the average of 0.50:0.00:0.2:0.3 and 0.20:0.30:0.50:0.00.

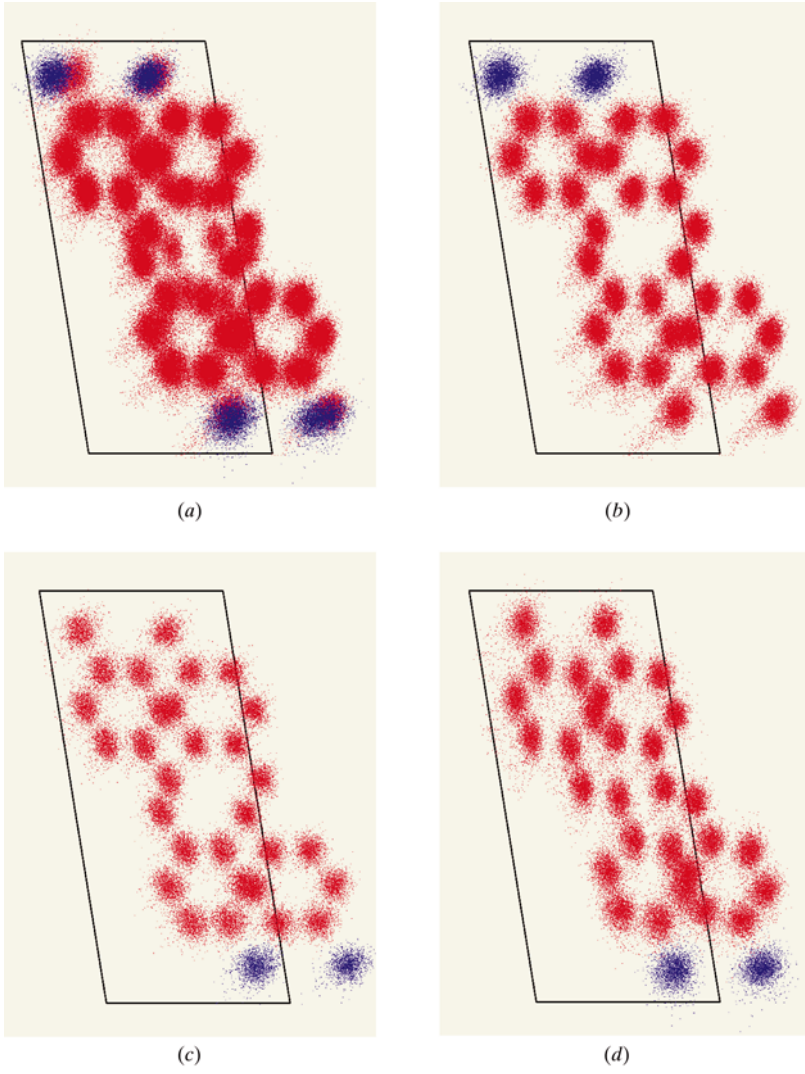

Figure 5
Plot of the average unit cell obtained by superposing on a single unit cell the positions of atoms from all unit cells in the MC simulation. Blue corresponds to the Cl atom, red to C atoms. (*a*) includes all molecular orientations. (*b*) Molecular orientations corresponding to $\sigma = +1$, $\rho = +1$ (50%). (*c*) Molecular orientations corresponding to $\sigma = -1$, $\rho = +1$ (20%). (*d*) Molecular orientations corresponding to $\sigma = -1$, $\rho = -1$ (30%). The refined cross-correlation parameter between σ and ρ resulted in there being 0% of the molecular orientation corresponding to $\sigma = +1$, $\rho = -1$.

4.2. Displacements induced by size-effect strain

With the parameters defining the occupational correlation structure fixed, refinement of the displacement variables was carried out using the parameters defining the spring model described earlier and summarized in Table 1. The eight spring constants K_i were initially all set to an arbitrarily chosen value of 100 in units of kT, where T is the simulation temperature and k is Boltzman's constant. All simulations were carried out with $kT = 1$. The size-effect parameters were set initially to 0.0 and allowed to refine subject to the constraint given by equation (10). Since the time taken for each simulation is directly proportional to the number of MC cycles, initially only 50 cycles of relaxation were used for each MC run, but in the later stages first 100 cycles and finally 200 cycles were used. It was found that the magnitude and shape of the stronger diffuse peaks close to the Bragg positions were not well modelled when only the smaller number of cycles was used, although the overall displacement patterns were similar. R factors for the agreement between observed and calculated patterns were ~3% less when 200 cycles of refinement were used compared with the best fit using only 50 cycles. Since by this stage a single MC simulation together with the accompanying calculation of its diffraction pattern took in excess of 2 h CPU time on a 400 MHz Pentium II processor, it was not feasible to increase the number of cycles per run any further.

During the early stages of the least-squares refinement, the spring constant K_5 became consistently very small or even slightly negative and the associated size-effect parameters therefore became meaningless. Consequently, for the remainder of the analysis K_5 was set to zero and refinement was carried out using parameters associated with the other seven springs, making a total of 28 refinable parameters or 29 when the occupancy cross-correlation parameter was included. In order to calculated the differentials necessary to form the least-squares matrix, it was necessary to perform MC simulations with the current set of parameters together with simulations in which each of the parameters in turn was incremented by a small amount. Thus, for each cycle of least-squares refinement, 30 individual MC simulations were required. These were carried out on a cluster of six 400 MHz Pentium II processors with the total time for a single least-squares cycle being about 11 h. The total CPU time required for refinement of the MC model was in excess of two weeks, although many times this amount of CPU time was utilized in developing and testing the model.

The final refined values for the force constants and size-effect parameters are given in Table 3. In Table 4, we list mean lengths and their r.m.s.

Table 2
Correlations of the occupancy variables used in the MC simulations.

No target correlations were specified corresponding to J_1 and J_2 since these interactions were not used in the refinement, *i.e.* it was assumed that $J_1 = J_2 = 0$.

MC energy constant	Target correlation	$\rho_{p,q,r,s}$	$\sigma_{p,q,r,s}$
J_1	–	−0.18	−0.20
J_2	–	−0.18	−0.21
J_3	−0.5	−0.43	−0.50
J_4	+0.225	+0.21	+0.23
J_5	+0.17	+0.16	+0.18
κ	Cross-correlation	+0.65	

deviations for all 26 intermolecular vectors that actually result in the simulation from the application of these size-effect parameters. The refined value for the cross-correlation parameter is given with the occupancy correlations in Table 2. The calculated diffraction pattern obtained from the final MC simulation is shown in Fig. 4(*c*) with the observed diffraction pattern plotted on the same scale given in Fig. 4(*d*) for comparison. Qualitatively, the comparison between observed and calculated patterns is good, though some small points of discrepancy may still be seen. The final overall *R* factor for the agreement,

$$R = \left(\chi^2 / \sum w I_{\rm obs}^2\right)^{1/2}, \qquad (11)$$

was 32.8% for 28530 data points. This agreement factor is substantially better than that obtained in a previous study of a PHTP inclusion compound (Mayo *et al.*, 1999), where it was considered that the 'guest' part of the structure was not adequately modelled, but is not as low as that achieved in the case of iron carbonyl (Welberry *et al.*, 1998). However, in that case only small regions of data containing the most significant features of the scattering were included in the analysis and it is quite likely that had the whole reciprocal-lattice sections been included an *R* factor comparable with the present one might have been obtained. In fact, at the early stage of the development of the methods described here, it is difficult to estimate exactly what level of agreement should be expected, since there are numerous possible sources of error, both random and systematic.

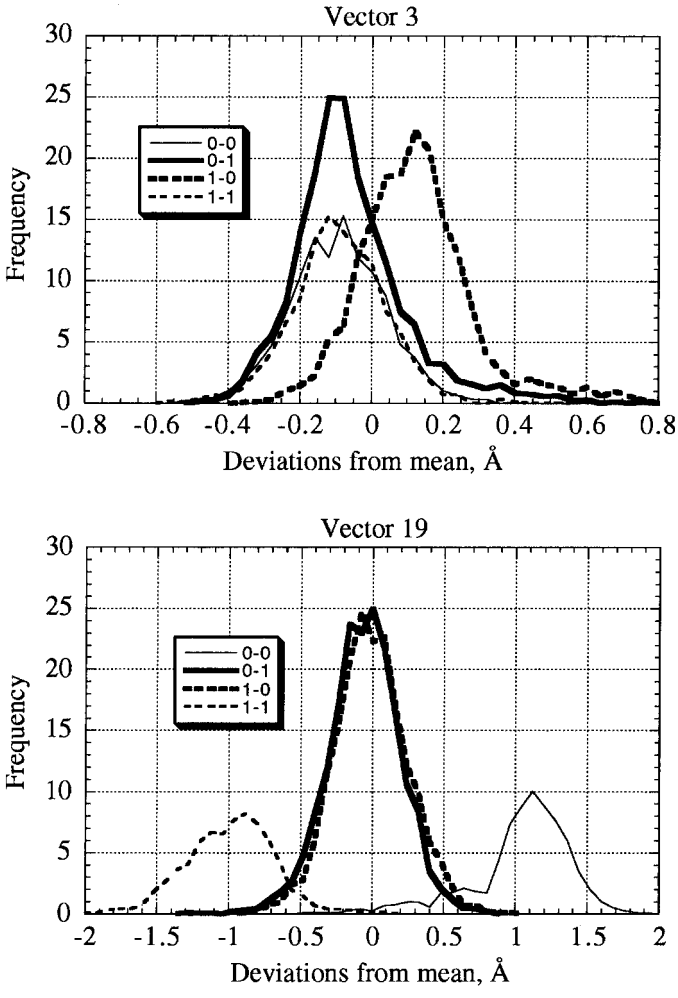

Figure 6
Plots of the distribution of vector lengths for two vectors, 3 and 19 (see Fig. 3), in the final MC simulation, as a function of the type of intermolecular vector, σ_n'–σ_m' = 0–0, 0–1, 1–0 or 1–1. In each case, the curve corresponding to the largest distance occurs when the contact is essentially between a Cl atom in one molecule with a Cl atom in the other.

Table 3
Values of the size-effect parameters, $\varepsilon_{0,0}$, $\varepsilon_{0,1}$, $\varepsilon_{1,0}$, $\varepsilon_{1,1}$, resulting from the least-squares refinement of the MC model.

The 8 different types of spring were placed on the 26 different vectors defined in Table 1 and resulted in the displacement distributions listed in Table 4. The force constant for spring 5 consistently refined to a very small value during early parts of the refinement and so was omitted during the later stages.

Spring	Force constant	$\varepsilon_{0,0}$	$\varepsilon_{0,1}$	$\varepsilon_{1,0}$	$\varepsilon_{1,1}$
1	131.8	0.1017	−0.0012	0.0054	−0.1063
2	437.1	−0.0426	−0.0149	0.0487	−0.0091
3	70.0	−0.3133	0.3023	0.4036	−0.5264
4	72.3	0.0434	0.1021	0.0421	−0.1330
5	0.0	0.0000	0.0000	0.0000	0.0000
6	272.2	0.4237	−0.0189	0.0063	−0.3880
7	77.8	0.0301	0.0706	−0.2134	0.0415
8	304.1	−0.0432	0.1584	−0.0594	−0.0257

4.3. Average structure

In Fig. 5(*a*), we show a plot of the projected average structure realized in the MC simulation. This was made by plotting in a single unit cell the coordinates of atoms from all unit cells in the structure. In Fig. 5(*b*), we similarly show a plot in which only molecules in the ($\sigma = +1$, $\rho = +1$) orientation are drawn, and in Figs. 5(*c*) and (*d*) corresponding plots for the ($\sigma = -1$, $\rho = +1$) and ($\sigma = -1$, $\rho = -1$) orientations. Note that the molecular orientation corresponding to ($\sigma = +1$, $\rho = -1$) was completely eliminated in the least-squares-fitting process.

It is quite noticeable that the average molecular site is not centrosymmetric so that to achieve overall centrosymmetry the derived realization must form domains in the crystal with the centrosymmetrically related structure equally represented. Since the diffraction data are centrosymmetric and therefore

Table 4
Distribution of distances (means and s.u.'s) along each of the 26 vectors used in the MC simulation.

Example plots of these distances can be seen in Fig. 6. In each case, the columns referred to as 0–0, 0–1, 1–0 and 1–1 correspond to the values of the end-to-end disorder variables, $\sigma'_{p,q,r,s}$, on the two molecules.

	0–0		0–1		1–0		1–1		All	
1	3.790	0.308	3.771	0.371	3.748	0.324	3.758	0.283	3.765	0.328
2	3.785	0.308	3.748	0.325	3.771	0.372	3.764	0.282	3.765	0.328
3	4.054	0.139	4.090	0.162	4.275	0.166	4.056	0.134	4.132	0.180
4	4.054	0.139	4.276	0.166	4.089	0.162	4.055	0.133	4.132	0.180
5	3.350	0.343	4.238	0.371	4.279	0.369	5.230	0.344	4.266	0.595
6	5.298	0.584	4.318	0.275	4.320	0.289	3.310	0.439	4.315	0.648
7	5.269	0.586	4.319	0.283	4.272	0.280	3.415	0.429	4.310	0.618
8	3.209	0.323	4.263	0.354	4.241	0.374	5.301	0.316	4.252	0.628
9	3.955	0.519	4.471	0.492	4.466	0.524	4.945	0.580	4.455	0.660
10	4.827	0.556	4.757	0.784	4.344	0.813	4.115	0.601	4.503	0.742
11	4.834	0.503	4.795	0.754	4.293	0.798	4.123	0.518	4.508	0.713
12	3.993	0.557	4.479	0.552	4.462	0.510	4.870	0.576	4.446	0.652
13	5.637	0.457	4.585	0.340	4.649	0.387	3.674	0.420	4.629	0.655
14	3.931	0.447	4.509	0.501	4.647	0.492	5.426	0.506	4.602	0.622
15	5.353	0.777	4.667	0.410	4.525	0.386	4.095	0.671	4.634	0.622
16	3.698	0.418	4.618	0.464	4.499	0.505	5.546	0.455	4.574	0.661
17	5.941	0.722	5.071	0.308	5.032	0.295	4.168	0.594	5.053	0.647
18	4.087	0.319	5.007	0.316	4.956	0.293	5.934	0.247	4.988	0.551
19	6.089	0.348	4.995	0.255	5.045	0.256	4.065	0.305	5.037	0.611
20	3.940	0.294	4.948	0.286	5.018	0.309	6.035	0.245	4.983	0.596
21	5.002	0.172	5.511	0.192	5.089	0.194	5.044	0.152	5.137	0.261
22	4.999	0.169	5.089	0.194	5.513	0.190	5.046	0.154	5.137	0.261
23	5.806	0.220	6.315	0.260	6.096	0.234	6.051	0.191	6.042	0.288
24	6.015	0.249	6.294	0.273	6.104	0.287	5.859	0.240	6.045	0.302
25	5.803	0.219	6.097	0.233	6.317	0.258	6.051	0.192	6.042	0.288
26	6.014	0.248	6.103	0.287	6.294	0.274	5.860	0.241	6.045	0.302

could not distinguish between two such structures, that we derived the one shown is quite fortuitous.

4.4. Local structure

The SRO parameters in Table 2, the force constants and 'size-effect' parameters in Table 3 and the resulting nearest-neighbour-distance distributions in Table 3 contain a great deal of information regarding the local structure. It is informative to take a closer look at some particular features.

The strong negative SRO correlation corresponding to J_3 reflects a tendency for the molecules to pack with neighbouring molecules head to tail, with the chlorine in one molecule more likely to be adjacent to the methyl group of its neighbour. If this nearest-neighbour tendency is allowed to progress naturally to the second neighbour, corresponding to the *a* cell-repeat interaction J_5, there would be a moderately strong positive correlation along this vector. For a simple Markov chain, a nearest-neighbour correlation of -0.5 would result in a second-neighbour correlation of $+0.25$. That the observed value for this correlation is only about $+0.17$ shows a strong direct second-nearest-neighbour interaction that is trying to oppose the effect of the nearest-neighbour forces. It is this low value for the J_5 correlation that gives the characteristic elongated diffuse peak shape seen in the diffraction patterns. Increasing the value of this correlation to 0.25 and beyond results in SRO peaks much more akin to those observed for MeCl (see Fig. 1*a*). The correlation structure observed within the layers of molecules in the *ab* plane is typical of a frustrated lattice, where nearest- and second-nearest-neighbour effects oppose each other.

In Fig. 6, we plot two examples of the distributions of intermolecular distances along vectors between neighbouring molecules. The distances plotted correspond to the distances between the pseudoatom sites 1 and 2 defining the end of the molecular motif. To a good approximation, these may be interpreted as describing the variations in distance between the Cl—Cl, Cl—Me and Me—Me distances in neighbouring molecules. For vector 3, the distance is greatest when the central molecule (see Fig. 3*b*) is in orientation $\sigma' = 1$ and the neighbouring molecule is in orientation $\sigma' = 0$. This in turn corresponds to the case when the contact is Cl—Cl. It appears that this 'size-effect' distortion is chiefly responsible for the strong asymmetry of the peaks labelled *A* in Fig. 1(*b*). Those symmetric peaks labelled *S* are close to a plane through the origin of reciprocal space and normal to vector 3. On this plane, the effects of displacements in the direction of vector 3 will be a minimum.

On vector 19, three quarters of the intersite vectors are of the type 0–1 or 1–0, which correspond to either Cl—Me or Me—Cl. The plots show that these distances cluster around the mean intersite distance. The relatively small number of intersite distances that are 0–0 or 1–1 (12.5% of each) are substantially longer or smaller, respectively. As for vector 3, the longer vectors correspond to the case where the contact is Cl—Cl.

5. Conclusions

In this paper, we have described a study of the X-ray diffuse scattering in the disordered molecular crystal system *p*-methyl-*N*-(*p*-chlorobenzylidene)aniline, using the recently developed method in which a Monte Carlo model of the structure is automatically fitted to the observed data *via* a least-squares technique. Despite the number of simplifications that it was necessary to make, a model involving only 4 short-range occupancy correlations, 7 intermolecular force constants and 21 'size-effect' parameters has been obtained, which gives generally good agreement between observed and calculated diffraction patterns, with an *R* factor of 32.8% (in intensities) for 28500 data points in a single section of reciprocal space.

The study represents a considerable computational problem that has stretched our current computational capabilities to the limit. By use of even greater computational resources, it is clear that a better solution could be found. There are a number of different ways in which further computational resources could be employed. First, it should be profitable to include more sections of diffuse data in the study. The MC model itself could also be substantially improved with a parameterization involving additional variables. In particular, it should be noted that, although the molecule has the potential of internal flexibility, this was neglected in the current study. It is possible that including a description of this internal flexibility alone could lead to significantly better agreement. A second area of improvement of the model would be to use 'size-effect' parameters that simultaneously depend on both side-to-side and end-to-end disorder. Further computational resources could also be employed to improve the quality of the computed diffraction patterns, by using larger simulation arrays and longer runs for calculating the diffraction patterns. Finally, it is expected that some further improvement could be obtained by using even larger numbers of cycles in the MC simulations.

Despite the compromises and simplifications that have had to be made, the present study has successfully shown that the refinable MC methodology can be made to work for even quite complex systems and has yielded detailed local ordering information not otherwise obtainable. With the ever increasing availabilty of fast and inexpensive computers, it is expected that the methodology will increasingly become viable as a means of analyis for a wide range of disorder problems.

I would like to thank Dr A. G. Christy for numerous helpful discussions during the course of this work, and Professor Joel Bernstein for first introducing me to the MeCl and ClMe systems.

References

Bar, I. & Bernstein, J. (1983). *Acta Cryst.* B**39**, 266–272.
Butler, B. D. & Welberry, T. R. (1992). *J. Appl. Cryst.* **25**, 391–399.
Haller, K. J., Rae, A. D., Heerdegen, A. P., Hockless, D. C. R. & Welberry, T. R. (1995). *Acta Cryst.* B**51**, 187–197.
Mayo, S. C., Proffen, Th., Bown, M. & Welberry, T. R. (1999). *J. Appl. Cryst.* **32**, 464–471.
Osborn, J. C. & Welberry, T. R. (1990). *J. Appl. Cryst.* **23**, 476–484.
Proffen, Th. & Welberry, T. R. (1997). *Acta Cryst.* A**53**, 202–216.
Warren, B. E., Averbach, B. L. & Roberts, B. W. (1951). *J. Appl. Phys.* **22**, 1493–1496.
Welberry, T. R. & Butler, B. D. (1994). *J. Appl. Cryst.* **27**, 205–231.
Welberry, T. R., Butler, B. D. & Heerdegen, A. P. (1993). *Acta Chim. Hung.* **130**, 327–345.
Welberry, T. R., Proffen, Th. & Bown, M. (1998). *Acta Cryst.* A**54**, 661–674.